

## Thermal model of water and CO activity of Comet C/1995 O1 (Hale-Bopp)

N. Gortsas<sup>a,\*</sup>, E. Kührt<sup>a,1</sup>, U. Motschmann<sup>a,b,2</sup>, H.U. Keller<sup>c,3</sup>

<sup>a</sup> Institute of Planetary Research, German Aerospace Center, Rutherford Str. 2, D-12489 Berlin, Germany

<sup>b</sup> Institute of Theoretical Physics, Technical University of Braunschweig, Mendelssohnstr. 3, D-38106 Braunschweig, Germany

<sup>c</sup> Institute for Geophysics and Extraterrestrial Physics, Technical University of Braunschweig, Mendelssohnstr. 3, D-38106 Braunschweig, Germany

### ARTICLE INFO

#### Article history:

Received 7 March 2010

Revised 9 January 2011

Accepted 14 January 2011

#### Keywords:

Comet Hale-Bopp

Comets, Nucleus

Comets, Composition

Thermal histories

Comets, Origin

Comets, Coma

### ABSTRACT

An investigation of the activity of Comet C/1995 O1 (Hale-Bopp) with a thermophysical nucleus model that does not rely on the existence of amorphous ice is presented. Our approach incorporates recent observations allowing to constrain important parameters that control cometary activity. The model accounts for heat conduction, heat advection, gas diffusion, sublimation, and condensation in a porous ice–dust matrix with moving boundaries. Erosion due to surface sublimation of water ice leads to a moving boundary. The movement of the boundary is modeled by applying a temperature remapping technique which allows us to account for the loss in the internal energy of the eroded surface material. These kind of problems are commonly referred to as Stefan problems. The model takes into account the diurnal rotation of the nucleus and seasonal effects due to the strong obliquity of Hale-Bopp as reported by Jorda et al. (Jorda, L., Rembor, K., Lecacheux, J., Colom, P., Colas, F., Frappa, E., Lara, L.M. [1997]. *Earth Moon Planets* 77, 167–180). Only bulk sublimation of water and CO ice are considered without further assumptions such as amorphous ices with certain amount of occluded CO gas. Confined and localized activity patterns are investigated following the reports of Lederer and Campins (Lederer, S.M., Campins, H. [2002]. *Earth Moon Planets* 90, 381–389) about the chemical heterogeneity of Hale-Bopp and of Bockelée-Morvan et al. (Bockelée-Morvan, D., Henry, F., Biver, N., Bois-sier, J., Colom, P., Crovisier, J., Despois, D., Moreno, R., Wink, J. [2009]. *Astron. Astrophys.* 505, 825–843) about a strong CO source at a latitude of 20°. The best fit to the observations of Biver et al. (Biver, N. et al. [2002]. *Earth Moon Planets* 90, 5–14) is obtained with a low thermal conductivity of  $0.01 \text{ W m}^{-1} \text{ K}^{-1}$ . This is in agreement with recent results of the Deep Impact mission to 9P/Tempel 1 (Groussin, O., A'Hearn, M.F., Li, J.-Y., Thomas, P.C., Sunshine, J.M., Lisse, C.M., Meech, K.J., Farnham, T.L., Feaga, L.M., Delamere, W.A. [2007]. *Icarus* 187, 16–25) and with previous thermal simulations (Kührt, E. [1999]. *Space Sci. Rev.* 90, 75–82). The water production curve matches the production rates well from –4 AU pre-perihelion to the outgoing leg while the model does not reproduce so well the water production beyond 4 AU pre-perihelion. The CO production curve is a good fit to the measurements of Biver et al. (2002) over the whole measured heliocentric range from –7 AU pre- to 15 AU post-perihelion.

© 2011 Elsevier Inc. All rights reserved.

### 1. Introduction

The long period Comet C/1995 O1 (Hale-Bopp) was discovered in July 1995 at a heliocentric distance of 7.2 AU. Its high intrinsic brightness already at 7 AU offered the unique opportunity to study the evolution of cometary activity over a wide range of heliocentric distances pre- and post-perihelion. The obtained data set of pro-

duction rates contains important information about the physical and chemical state of the nucleus. Thermophysical nucleus models provide a means to access this information by matching calculated production rates to those derived from observations. In particular, measurements of the nuclear activity over a wide range of heliocentric distances pre- and post-perihelion strongly constrain the model assumptions and parameters. Near the Sun the absorbed energy is mainly used to maintain cometary activity while at larger heliocentric distances when the activity subsides the fractions of energy going to re-radiation and transfer into the nucleus interior become dominant.

Comet Hale-Bopp has been studied with a wide range of instruments. A good overview of the employed techniques and a discussion of the early understanding of the observations can be found in Bockelée-Morvan and Rickman (1997). From ground-based radio

\* Corresponding author. Fax: +49 30 67055 386.

E-mail addresses: [Nikolaos.Gortsas@dlr.de](mailto:Nikolaos.Gortsas@dlr.de) (N. Gortsas), [Ekkehard.Kuehrt@dlr.de](mailto:Ekkehard.Kuehrt@dlr.de) (E. Kührt), [Uwe.Motschmann@tu-bs.de](mailto:Uwe.Motschmann@tu-bs.de) (U. Motschmann), [keller@linmpi.mpg.de](mailto:keller@linmpi.mpg.de) (H.U. Keller).

<sup>1</sup> Fax: +49 30 67055 386.

<sup>2</sup> Fax: +49 531 391 5833.

<sup>3</sup> Fax: +49 531 391 5220.

telescopes production rates for a variety of species were derived. A progressive release pattern for species like CO, CH<sub>3</sub>OH, HCN, H<sub>2</sub>O (from OH) and many others along the incoming branch has been detected (Jewitt et al., 1996; Biver et al., 1997). In addition, water production rates have been contributed by other groups (Colom et al., 1997; Stern et al., 1999; Weaver et al., 1999; Crovisier et al., 1999). Biver et al. (2002) updated their observations twice summarizing in their 2002 publication the full set of observations covering a heliocentric distance from –7 AU pre- to 15 AU post-perihelion.

Among the first who studied Comet Hale-Bopp with a thermal model was Prialnik (1997a). The model assumed that 5% of CO gas is occluded in an amorphous ice matrix. The calculated CO curve after perihelion is almost constant in contradiction with CO observations. A similar result was reported by Flammer et al. (1999) who also obtained an almost flat CO curve. Their model assumed that there are H<sub>2</sub>O clathrate grains with occluded CO gas. However, the observations of Jewitt et al. (1996) and Biver et al. (1997) show a peak in CO production around perihelion. Later, Prialnik (1997b) presented a thermal model to study the long-term evolution of Hale-Bopp. A key model assumption is the existence of amorphous water ice with occluded CO gas. But the model does not resolve the diurnal rotation of the comet. At that time, only few pre-perihelion observations were available.

Enzian et al. (1998) presented a thermal model of Hale-Bopp and compared their results for water and CO with pre-perihelion observations. Key model assumptions are the existence of amorphous ice with occluded CO gas. A modest fit to the available data points of CO was achieved by assuming 10% of CO occluded in amorphous ice, 0° obliquity of the rotation axis, and an argument of the sub-solar meridian of 0°. The water observations could not be fitted prior to 4 AU pre-perihelion. An estimate of the possible contribution of an extended water source due to water ice sublimation from icy grains in the coma is given. The proposed estimate allows to fit the data points beyond 4 AU. On the post-perihelion branch, however, it is apparent that the water contribution of the extended source exceeds the observations. When the data set of Biver et al. (1997) became available, Enzian (1999) applied again his thermal model on Hale-Bopp. He considered two different values of the obliquity of the rotation axis 0° and 90°. The chemical composition of the comet was made up with 50% mass of dust, 40% amorphous water ice, 5% CO trapped in amorphous water ice, and 5% CO ice as an independent phase. With these assumptions the author was able to reproduce the pre-perihelion CO outgassing pattern with an obliquity of 90°. The fit of the CO data along the post-perihelion branch is modest and ends at 4 AU post-perihelion. The data fit with 0° obliquity of the rotation axis was poor pre- and post-perihelion. At the same time, the water production rates could not be fitted beyond 4 AU pre-perihelion.

Kührt (1999) showed that a thermophysical nucleus model is able to match the water sublimation measurements without the assumption of extended water sources in the coma. Based on the strong obliquity of Hale-Bopp as reported by Jorda et al. (1997), Kührt (1999) investigated the apparently strong influence of seasonal effects on the water sublimation curve. He showed that it is possible to fit the water production rates if a low thermal conductivity is used.

Capria et al. (2000) published a thermal model of Comet Hale-Bopp and compared their results with CO observations in the range from –7 AU pre- to 3 AU post-perihelion. The best fit to the data set which was available at that time was achieved by assuming that CO exists as an independent ice phase and that 20% of the CO is released only after water sublimation. Another 10% of the CO gas is trapped in amorphous ice. In a later article, Capria et al. (2002) compared their results for the water and CO activity of Hale-Bopp with observations in the range from –7 AU pre-

4 AU post-perihelion. The calculated water flux fits the observations only in the range from –2 AU to –1 AU, pre-perihelion. The remaining data points in the range from –5 AU to –2 AU are not fitted by the model, neither are the data points along the post-perihelion branch. The assumptions of the trapped CO ice are similar to those of Capria et al. (2000). In the range from –2 AU to –1 AU the fit to the CO data is good as in Capria et al. (2000). In the range from –7 AU to –2 AU the curve is an upper limit to the observations. The same holds for the post-perihelion branch. The range covered along the post-perihelion branch is 1–4 AU. The curve does not match the data points so well.

It can be concluded that the models of Enzian (1999) and Capria et al. (2002) fit the observations of Hale-Bopp for CO quite well although neither model has been applied to the full data set covering a range from –7 AU pre- to 15 AU post-perihelion as reported by Biver et al. (2002). Both models employ similar assumptions on the existence of amorphous ice and the amount of occluded CO gas (5–20%). The water production curve could not be reproduced so well by either model. Both suggest that extended sources might be responsible for the water sublimation beyond 4 AU pre-perihelion.

In this article, a thermal model is presented and applied to Comet Hale-Bopp which relies only on the assumption of CO ice bulk sublimation and on seasonal effects. Confined and localized activity of water and CO ice is studied following recent observational evidences on important properties of comets (Lederer and Campins, 2002; Groussin et al., 2007; Bockelée-Morvan et al., 2009) and earlier results of Kührt (1999) on the importance of seasonal effects and a low thermal conductivity. Amorphous ice is not included in the model calculations. Its existence in comets is still under discussion (Huebner, 2009). The model solves the heat and mass transfer problem for cometary activity with a sophisticated method to deal with moving boundaries. Heat conduction, heat advection, gas diffusion, sublimation and condensation are taken into account. The movement of the surface boundary is implemented following the concept of Crank and Gupta (1972). This kind of moving boundary problems are referred to as Stefan problems (Crank, 1984). The model is applied to the full data set of water and CO production rates covering a range from –7 AU pre- to 15 AU post-perihelion as reported by Biver et al. (2002).

The article is organized as follows: The thermal model is introduced in Section 2. A collection of recent observational findings are given at the beginning of Section 3. The simulation results follow this discussion. In Section 4 conclusions are drawn.

## 2. Model description

### 2.1. Thermal model

Our model comet consists of water ice, CO ice, dust and pores. Further components can principally be added. The model solves the coupled heat and mass transfer problem with moving boundary conditions.

In a volume element energy is transported through heat conduction of the ice matrix, heat advection of the vapor, and sublimation or condensation processes in the pores. A theoretical description of these processes starts with the general formulation of the conservation laws of mass, momentum, and energy as appropriate for comets. Mass conservation is expressed through a balance equation for the vapor mass density  $\rho_\mu$  and the solid ice mass density  $\rho_\mu^s$  of species  $\mu$

$$\frac{\partial \rho_\mu}{\partial t} + \nabla \cdot (\rho_\mu u_\mu) = - \frac{\partial \rho_\mu^s}{\partial t}, \quad (1)$$

and

$$\frac{\partial \rho_{\mu}^s}{\partial t} = -q_{\mu}. \quad (2)$$

$x$  and  $t$  denote the spatial and temporal coordinates.  $u_{\mu}$  denotes the diffusion velocity of the  $\mu$  volatile component. The source term  $q_{\mu}$  defines bulk evaporation. Following Mekler et al. (1990) it can be calculated as the difference between the gas density  $\rho_{\mu}$  of species  $\mu$  in the pores and the equilibrium state  $\rho_{\mu,eq}$  at some bulk temperature  $T$

$$q_{\mu} = f_p(\rho_{\mu,eq} - \rho_{\mu})c_{th,\mu}(T). \quad (3)$$

Here  $c_{th,\mu}$  denotes the mean thermal velocity of the  $\mu$  gas species and  $f_p$  is a factor that depends on structural properties of the comet, e.g.  $f_p = 2\psi/r_p$  with  $\psi$  being the porosity and  $r_p$  the effective pore radius. In this model the pores are modeled as cylindrical capillaries whose circular cross-section has a diameter of  $2r_p$  (Mekler et al., 1990). The  $\rho_{\mu,eq}$  is given by the vapor pressure which is calculated with the Clausius–Clapeyron equation and the assumption that the gas obeys the ideal gas law

$$\rho_{\mu,eq} = \frac{P_{v,\mu}m_{\mu}}{k_B T}. \quad (4)$$

$m_{\mu}$  and  $k_B$  denote the mass of species  $\mu$  and the Boltzmann constant, respectively. The saturation pressure  $P_{v,\mu}$  is given according to the empirical formula of Fanale and Salvail (1984) as  $P_{v,\mu}(T) = A_{\mu}\exp(-B_{\mu}/T)$ . The values of the constants can be found in Table 1. An implicit assumption of this approach is that there is bulk ice in the pores so that the reference state can prevail.

The mean free path of molecules exceeds the characteristic length scale of a porous nucleus, e.g. the lengths characterizing the structure of the pores. Therefore, the Knudsen number is much larger than 1. In this case the vapor velocity field can be calculated from the Knudsen formula

$$\rho_{\mu}u_{\mu} = -C_{\mu}\frac{\partial}{\partial x}(\rho_{\mu}\sqrt{T}). \quad (5)$$

$C_{\mu}$  is a factor that can be related to structural and thermal parameters (Benkhoff and Spohn, 1991), e.g.  $C_{\mu} = 2\psi r_p c_{th,\mu}$ .

Eqs. (1) and (5) describe the diffusion of vapor inside a predefined porous structure in a macroscopic model. The conservation of energy written in terms of temperature under the assumptions of a Fourier type heat flux, the advection of energy through vapor flow, and an energy source term reads as, e.g. Spohn and Benkhoff (1990),

$$c\rho\frac{\partial T}{\partial t} + \sum_{\mu} c_{g,\mu}\rho_{\mu}u_{\mu}\frac{\partial T}{\partial x} = \frac{\partial}{\partial x}\kappa\frac{\partial T}{\partial x} - \sum_{\mu}\Delta H_{\mu}q_{\mu}. \quad (6)$$

**Table 1**  
Basic parameters.

Quantity	Symbol	Value
Density of water ice	$\rho_i$	917 kg/m <sup>3</sup>
Specific heat of water ice	$c_i$	1610 J/(kg K)
Specific heat of water gas	$c_{g,i}$	1370 J/(kg K)
Pressure constant water ice	$A_i$	$3.56 \times 10^{12}$ Pa
Temperature constant water ice	$B_i$	6141.667 K
Thermal enthalpy of water ice	$\Delta H_i$	$2.84 \times 10^6$ J/kg
Density of CO ice	$\rho_{co}$	1250 kg/m <sup>3</sup>
Specific heat of CO ice	$c_{co}$	2010 J/(kg K)
Specific heat of CO gas	$c_{g,co}$	720 J/(kg K)
Pressure constant CO ice	$A_{co}$	$1.2361 \times 10^9$ Pa
Temperature constant CO ice	$B_{co}$	764.16 K
Thermal enthalpy of CO ice	$\Delta H_{co}$	$0.227 \times 10^6$ J/kg
Density of dust	$\rho_d$	3000 kg/m <sup>3</sup>
Specific heat of dust	$c_d$	1300 J/(kg K)
Emissivity	$\epsilon_{em}$	0.96
Bond albedo	$\mathcal{A}$	0.04

$c_{g,\mu}$  denotes the specific heat of vapor of species  $\mu$ . It is calculated by assuming the validity of the ideal gas law for water and CO vapor. Dust enters the model via  $c\rho = \sum_{\mu}c_{\mu}\rho_{\mu}$ .  $\rho_{\mu}$  denotes the bulk density of species  $\mu$  which equals  $\rho_{b,\mu}\gamma_{\mu}$ .  $\rho_{b,\mu}$  and  $\gamma_{\mu}$  denote the solid bulk velocity and the volumetric filling factor of species  $\mu$ . The sum goes over all constituents of the material, e.g. solid and vapor. It reduces the active surface fraction with respect to pure porous ice (Davidsson and Skorov, 2002b).

The description is one dimensional with respect to the processes taking place inside the nucleus. But the boundary condition accounts for different irradiation patterns which allows us to consider active surface areas throughout the comet surface. The one dimensional description is justified because the lateral components of the thermal conduction coefficient are assumed to be small compared to the radial direction, see also the discussion below on the thermal conduction coefficient. In addition, processes related to cometary activity are believed to be confined in the range of few cm to meters. This is small compared to the radius of a comet of several km size. Therefore, it is safe to employ the plane parallel approximation.

Energy transport through heat conduction in the ice matrix is described by the first term on the right hand side of Eq. (6). Its contribution to the energy budget depends heavily on the choice of the thermal conduction coefficient  $\kappa$  which describes energy transport in the solid phase (grains and ices). It depends on the structure and composition of cometary material and it is sometimes assumed to be temperature dependent. Some authors also include radiative heat transfer to  $\kappa$  but at temperatures typical for comets it can be neglected. Steiner and Kömle (1991) presented an approach to add the heat transport by vapor flux through the pores to the thermal conduction coefficient  $\kappa$ .

On the experimental side, there are studies of the thermal conductivity of porous ice in connection with comets. For a review on various measurements, especially for water ice phases, consult Seiferlin et al. (1996) and Seiferlin (1991) and the bibliography therein.

However, many unsolved questions like the existence of amorphous ice or the porosity and pore size distribution in cometary nuclei make it difficult to derive realistic values. Laboratory measurements (Spohn et al., 1989; Seiferlin, 1991; Grün et al., 1993; Stöffler et al., 1991) generally suffer from the widely unknown structure and composition of cometary matter and may not be representative. We, therefore, developed a model that tries to keep the number of free parameters as low as possible by incorporating what is currently known based on recent observations of and missions to comets (Jorda et al., 1997; Fernández, 2002; Lederer and Campins, 2002; Groussin et al., 2007; Bockelée-Morvan et al., 2009).

## 2.2. Characteristic time scales

We perform a thorough analysis of the relevant time scales to evaluate the importance of the terms in Eq. (1) (Spohn and Benkhoff, 1990). The analysis is carried out for water vapor but is equally applicable to CO vapor. We therefore drop the  $\mu$  index. The characteristic time scales of heat conduction  $\tau_h$  and gas diffusion  $\tau_g$  can be expressed as

$$\tau_h = \frac{L^2\rho c}{\kappa} \quad (7)$$

and  $\tau_g$  as

$$\tau_g = \frac{L^2}{C\sqrt{T}}. \quad (8)$$

$L$  denotes a characteristic length scale of the problem. It cannot exceed the mean free path of the vapor molecules because then the

flow is deviating from the free molecular flow regime. In case that the pores are modeled to be cylindrical tubes  $L$  describes the length of the pores while the previously introduced pore radius  $r_p$  describes the radius of their cross-section.

All quantities in Eq. (1) are scaled to dimensionless quantities which are indicated by a \* superscript. Time is referred to the heat time scale  $t^* = t/\tau_h$ . The depth  $x$  is scaled to  $L$ , e.g.  $x^* = x/L$ . The vapor density is scaled to an equilibrium value at the surface temperature of a water ice covered nucleus at perihelion  $\rho^* = \rho/\rho_{eq}$ . The velocity field is scaled to the thermal velocity at the surface temperature at perihelion, e.g.  $u^* = u/c_{th}$ . The mass source term which describes the change of vapor density with time is scaled to the ratio of the vapor density reference value  $\rho_{eq}$  and the time scale of gas diffusion  $\tau_g$ , e.g.  $q^* = q\tau_g/\rho_{eq}$ . Mapping of Eq. (1) to dimensionless quantities leads then to

$$\frac{\tau_g}{\tau_h} \frac{\partial \rho^*}{\partial t^*} + \frac{\tau_g c_{th}}{L} \frac{\partial(\rho^* u^*)}{\partial x^*} = q^*. \quad (9)$$

Entering the expressions of the characteristic scales leads to

$$\frac{\kappa}{\rho c 2\psi c_{th}} \frac{1}{r_p} \frac{\partial \rho^*}{\partial t^*} + \frac{1}{2\psi} \sqrt{\frac{L^3}{r_p^3}} \frac{\partial(\rho^* u^*)}{\partial x^*} = q^*. \quad (10)$$

The coefficient of the time derivative is only significant for very small pore radii, e.g.  $r_p < 10^{-8}$  m. For typical pore sizes of comets in the range of a few to 100  $\mu\text{m}$  it is thus safe to neglect the temporal variations of the vapor density. We therefore solve the mass conservation equation Eq. (1) without the temporal variation of the mass density yielding

$$\nabla(\rho_\mu u_\mu) = q_\mu. \quad (11)$$

The obtained set of coupled equations is then solved numerically on a grid that is modified according to the techniques discussed below.

### 2.3. Boundary conditions

The heat transfer equation is closed by appropriate boundary conditions. At the surface the energy balance equation in the unit  $\text{W m}^{-2}$  provides a commonly used boundary condition which is only very briefly discussed here

$$\frac{F_{S,0}}{r_H^2(t)} (1 - \mathcal{A}) \max_{\zeta \in [0, 2\pi]} \{0, \cos(\zeta)\} = \epsilon_{em} \sigma T^4 + \kappa \nabla T(x, t) + Q(T) + \sum_{\mu} c_{g,\mu} \rho_\mu u_\mu T. \quad (12)$$

The left hand side of the equation describes the solar irradiation of the surface at some heliocentric distance  $r_H$ .  $F_{S,0}$  is the solar constant,  $\mathcal{A}$  the Bond albedo, and  $\zeta$  the solar zenith distance.  $\epsilon_{em}$  and  $\sigma$  are the thermal emissivity and the Stefan–Boltzmann constant, respectively. The angle  $\zeta$  is important since it controls how the incoming solar energy is distributed over the surface of the nucleus. It is calculated according to the following formulas (Sekanin-a, 1979):

$$\cos(\zeta) = \cos(\theta) \cos(\phi) \cos(\theta_s) + \sin(\theta) \sin(\theta_s) \quad (13)$$

$\theta$  is the latitude,  $\phi$  the hour angle, and  $\theta_s$  the cometocentric latitude of the sub-solar point.  $\theta_s$  is given by

$$\sin(\theta_s) = \sin(\delta) \sin(\Phi + \alpha). \quad (14)$$

$\delta$  is the obliquity and  $\Phi$  the argument of the sub-solar meridian at perihelion. The true anomaly  $\alpha$  of the comet is calculated by using Kepler's equations. The terms on the right hand side of Eq. (21) describe surface reemission due to the Stefan–Boltzmann law, thermal conduction between the surface and the nucleus, surface ice sublimation, and energy transport from the gas phase. In our model the

nucleus surface is covered by water ice of volume fraction  $f_i$  and dust. The orientation of our coordinate system is such that  $x = 0$  denotes the surface of the nucleus and  $x = x_b$  the bottom. The surface sublimation term is given by the Hertz–Knudsen formula

$$Q_\mu(T) = f_\mu \Delta H_\mu P_{v,\mu}(T) \sqrt{\frac{m_\mu}{2\pi k_B T}} \quad (15)$$

The lower boundary is given by the constraint that the thermal flux vanishes

$$\kappa \nabla T(x_b, t) = 0. \quad (16)$$

This adiabatic approach expresses the assumption that a quasi-stationary state is reached in a rotating body at depths beyond many diurnal skin depths of the thermal wave. Depending on the value of the thermal conductivity the position of the lower boundary has been chosen to secure a vanishing thermal flux well above the lower boundary.

A boundary condition for the gas diffusion problem is difficult to obtain, see e.g. the discussion in Skorov et al. (2001) and Davids-son and Skorov (2004). At this stage, we follow the approach of most groups and set the vapor density equal to zero at the surface for CO, see e.g. Mekler et al. (1990)

$$\rho_{co}(x = 0) = 0. \quad (17)$$

For water vapor we follow Spohn and Benkhoff (1990) and set its value to the equilibrium conditions at the given surface temperature  $T_s$

$$\rho_v(x = 0) = \rho_{v,eq}(T_s). \quad (18)$$

### 2.4. Stefan problem of comets

The thermal evolution of comets needs to be treated as a Stefan problem if the thermal conductivity is low ( $< 0.1 \text{ W m}^{-1} \text{ K}^{-1}$ ). In this case, the propagation velocity of the diurnal heat wave

$$v_p = \sqrt{\frac{4\pi\kappa}{\rho c \tau_r}} \quad (19)$$

is comparable to the erosion velocity of surface material  $v_e = Q/(\Delta H \rho_i)$  at perihelion.  $\tau_r$  is the diurnal rotation period. Taking typical values for water ice at perihelion shows that both velocities are of the same order, e.g.  $\approx 6 \times 10^{-7}$  m/s. Hence, the penetration of the nucleus by the diurnal heat wave is obstructed. This effect needs to be resolved by treating the thermal evolution as a Stefan problem.

The set of equations presented in the previous section, i.e. Eqs. (1), (5), and (6) and its boundary conditions, has to be extended in order to incorporate surface erosion into the model. Due to sublimation of water ice a certain amount of surface material is ejected into space. Hence, the upper boundary is moving as sketched in Fig. 1. This movement poses a challenge to numerical modeling especially to the calculation of the thermal gradient in Eq. (21). In general, the thickness of the eroded surface layer  $\Delta s$  deviates from the spatial discretization size  $\Delta x$ . As a result the distance between the actual location of the surface boundary and the next grid node is less than  $\Delta x$ . In finite-difference schemes there are several approaches to deal with this situation (see Crank, 1984). Our approach is motivated by the work of Crank and Gupta (1972). The thickness of the eroded surface layer  $\Delta s_\mu$  of species  $\mu$  is obtained from the so called Stefan condition (Stefan, 1891)

$$\frac{\Delta s_\mu}{\Delta t} = \frac{Q_\mu(T)}{\Delta H_\mu \rho_\mu}. \quad (20)$$

The spatial grid  $\Gamma$  is moved according to this erosion size  $\Delta s$  at each time step, see Fig. 2. The temperature field is obtained at the

new grid  $\Gamma^*$  through interpolation by cubic splines. The cubic splines  $S_j(x)$ , with  $j$  counting the number of intervals in the old grid  $\Gamma$ , are given by

$$S_j(x) = s_{j,0} + s_{j,1}(x - x_j) + s_{j,2}(x - x_j)^2 + s_{j,3}(x - x_j)^3. \quad (21)$$

The coefficients  $s_{j,*}$  are obtained from a set of continuity conditions up to second order taken at the cell boundaries.  $x_j$  denotes the coordinate of the left sided edge of the interval  $j$ . Once the cubic spline functions are known the temperature at the new grid  $\Gamma^*$  is obtained through

$$T(x_j^*, t) := S_j(x_j + \Delta s, t). \quad (22)$$

The adaptation of the spatial grid will be called temperature remapping. At each time step the erosion of surface material is taken into account. It is introduced to ascertain a constant spatial discretization despite surface erosion. It is designed to secure that the upper boundary is located on a grid node at each time step. Besides loss of energy through surface sublimation and thermal emission the nucleus is also losing the internal energy of the eroded surface material.

The mass and flux densities are only linearly interpolated to the new grid. Numerical calculations have shown that for the gas density a higher accuracy is not as important as for the temperature which controls the amount of energy entering the nucleus. This approach also reduces the amount of computing time considerably.

### 2.5. Grid adaptation

In comets sublimation does not only occur at the surface but also in the interior. In this article an additional volatile species sublimating from the interior is considered, e.g. CO. While the situation at the surface remains as in the previous section, the fact that there is a volatile species in the interior leads to a moving material interface. Therefore, the depth of the CO front denoted by  $A_{co}$  is time dependent. The number of grid nodes  $N_A(t)$  distributed over  $A_{co}$  is obtained from

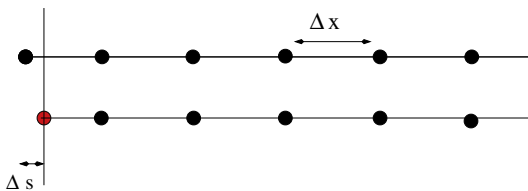


Fig. 1. Due to surface sublimation a certain amount of material is ejected from the surface of the nucleus. This leads to a moving boundary and to a deviation between the actual grid and the current position of the surface. Special techniques are necessary for a proper treatment.

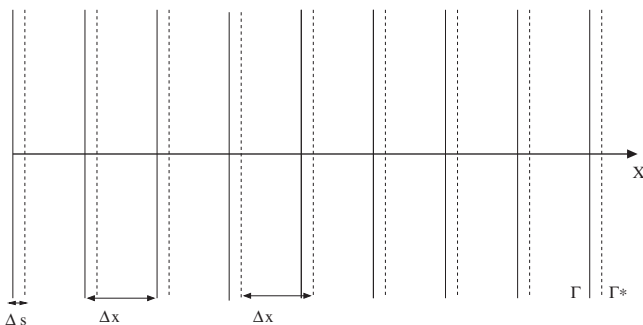


Fig. 2. The spatial discretization size  $\Delta x$  remains constant throughout the computation. The old grid  $\Gamma$  is moved according to the erosion of surface material  $\Delta s$ . The temperature field at the new grid  $\Gamma^*$  is obtained through interpolation with cubic splines (Crank and Gupta, 1972).

$$N_A(t) = \frac{A_{co}(t)}{\Delta x}. \quad (23)$$

$\Delta x$  is the spatial discretization size, which is kept constant throughout the computation. Initially, the material interface is located on a grid node which means that  $N_A(t)$  is an element of  $\mathbf{N}$ , the set of all positive integers,

$$N_A(t) \in \mathbf{N}. \quad (24)$$

In general, CO sublimation leads to a violation of this condition. The movement of the CO front is resolved by first solving Eq. (20) for CO. Second, the amount of surface erosion  $\Delta s_i(t)$  and the movement of the CO front  $\Delta s_{co}(t)$  is collected for several time steps, e.g.  $t_1, \dots, t_N$ ,

$$A_{co}(t_N) = \sum_{j=1}^N (A_{co}(t_{j-1}) + \Delta s_{co}(t_j) - \Delta s_i(t_j)). \quad (25)$$

Once the CO front  $A_{co}(t)$  exceeds a grid node from the surface away, the number of grid nodes distributed along  $A_{co}(t)$  is increased by 1. In the opposite case, the CO front  $A_{co}(t)$  exceeds a grid node towards the surface leading to a reduction of the grid nodes distributed over  $A_{co}$  by 1. Depending whether surface erosion or CO sublimation dominates, the number of grid points between the surface and the CO front will decrease or increase with time. This approach has the benefit to be robust but it does not resolve the actual location of the inner front below the spatial discretization size  $\Delta x$ . It assumes that the CO front remains all the time on a grid node as long as the number of grid nodes does not change according to the described method. This approach is checked against variations of the spatial discretization size and it fulfills the appropriate stability conditions.

### 2.6. Summary of model assumptions

Based on the arguments given above and on additional numerical studies we start from the following list of assumptions (which is not exhaustive):

- The heat conductivity of cometary matter is low and, therefore, a careful treatment of the thermal evolution of the comet as a Stefan problem is important.
- Heat conduction, heat advection, gas diffusion, sublimation, and condensation processes are considered.
- Amorphous ice is not included in the model. Its existence in comets is still under discussion (Huebner, 2009).
- Dust enters implicitly into this model via the material parameters specific heat, density, and thermal conductivity. We further assume that all dust grains that are liberated from the ice matrix at the surface are carried into the coma by the gas flow, i.e. dust mantle formation is assumed not to take place. Although dust mantle formation appears common among less active comets, the current assumption may be realistic for a highly active comet like Hale-Bopp.

## 3. Results

### 3.1. Calculation setup

The nucleus model of Hale-Bopp assumes a two-layer stratigraphy with the upper layer being a mixture of water ice and dust while the lower layer includes also CO ice. The parameters of the calculations can be found in Tables 1–4.

Comet Hale-Bopp is a long period comet with a period of 2500 years. CO and water activity, however, occur when the comet is close to the Sun. Therefore, for this study the comet is put at a heliocentric distance of 20 AU and the calculations proceed from

there to 20 AU post-perihelion. This approach was also followed by Enzian et al. (1998) and Enzian (1999).

### 3.2. Observational findings

An important input parameter for the thermal evolution of a comet is the thermal conductivity. Groussin et al. (2007) analyzed the near infrared spectra of the Deep Impact mission to Comet 9P/Tempel 1. From these data a low thermal inertia of  $\leq 50 \text{ W K}^{-1} \text{ m}^{-2} \text{ s}^{1/2}$ , corresponding to a heat conductivity less than  $0.003 \text{ W K}^{-1} \text{ m}^{-1}$ , was derived. In addition, Kührt (1999) showed for Comet Hale-Bopp that a thermophysical nucleus model with a low thermal conduction coefficient of  $0.001 \text{ W K}^{-1} \text{ m}^{-1}$  is able to reproduce the water sublimation measurements by assuming solely water ice sublimation without further assumptions, such as extended sources (Enzian et al., 1998). More recently, Davidsson et al. (2009) re-evaluated the infrared spectra of the Deep Impact mission to Comet 9P/Tempel 1. They included surface roughness into the model and derived thermal inertia values for most surface areas (inactive surface elements) in the range of  $1000\text{--}3000 \text{ W K}^{-1} \text{ m}^{-2} \text{ s}^{1/2}$  or about  $1\text{--}10 \text{ W K}^{-1} \text{ m}^{-1}$ . Due to the uncertainty of  $\kappa$  we investigated several cases from  $0.001 \text{ W K}^{-1} \text{ m}^{-1}$  to  $0.1 \text{ W K}^{-1} \text{ m}^{-1}$ . The best fit to the observations was obtained with a  $0.01 \text{ W K}^{-1} \text{ m}^{-1}$  which is employed for all presented figures of this paper.

The radius of the comet was set to 30 km as reported by Fernández (2002). Jorda et al. (1997) put the diurnal rotation time of Hale-Bopp to a value of 11.4 h.

Another important input parameter is the obliquity of the rotation axis. The distribution of the incoming solar energy on the surface of the comet heavily depends on this parameter as can be

**Table 2**  
Set of model parameters.

Quantity	Symbol	Value
Mass concentration of water ice	$X_i$	0.4
Mass concentration of CO ice	$X_{co}$	0.1
Mass concentration of dust	$X_d$	0.5
Porosity	$\psi$	0.5
Pore radius	$r_p$	100 $\mu\text{m}$

**Table 3**  
Orbital and rotational parameters of Hale-Bopp. JPL denotes the NASA Small-Body Database.

Quantity	Symbol	Value	Source
Eccentricity	$\epsilon$	0.9950817161	JPL
Semi-major axis	$a_{semi}$	185.864 AU	JPL
Diurnal rotation period	$\tau_r$	11.4 h	Jorda et al. (1997)
Orbital rotation period	$t_{orb}$	2500 year	JPL
Obliquity of the rotation axis	$\delta$	84°	Jorda et al. (1997)
Argument of sub-solar meridian	$\Omega$	105°	
Nucleus radius	$R$	30 km	Fernández (2002)

**Table 4**  
Numerical parameters.

Quantity	Symbol	Value
Temporal discretization	$\Delta t$	200 s
Spatial discretization	$\Delta x$	1 mm
Depth of lower boundary	$x_b$	5 m
Initial depth of the CO front	$x_{CO}$	50 cm

inferred from Eqs. (13) and (14). Following Sekanina (1979), the illumination of a surface area can be calculated if the obliquity and the argument  $\Phi$  of the sub-solar meridian at perihelion are known. Jorda et al. (1997) published a value for the obliquity of Hale-Bopp of about 84°. This value was used in Kührt (1999) together with an argument  $\Phi$  of 64° which is slightly below the lower range provided by Vasundhara and Chakraborty (1999). Enzian et al. (1998) set  $\Phi$  to 0° which was probably also employed in Enzian (1999). Vasundhara and Chakraborty (1999) calculated the obliquity and the argument of the sub-solar meridian at perihelion. They published eight values for dates between October 6, 1996 and October 9, 1997 covering ranges from 77° to 90° for the obliquity and from 68° to 84° for the argument  $\Phi$ . It seems that these angles are not so well constrained. We, therefore, put the obliquity to a value of 84° which was also published in Jorda et al. (1997) and considered several values for the argument  $\Phi$ . It turned out that our simulations favor a value of 105°.

In their recent paper Bockelée-Morvan et al. (2009) indicate that strong compositional inhomogeneities might be present at Hale-Bopp particularly for CO sources. The investigators report about a CO jet at a latitude position of 20° from which 40% of the observed outgassing may originate. Finally, Bockelée-Morvan et al. (2009) also report about the lack of a correlation between the CO jet and dust jets. Earlier, Lederer and Campins (2002) also wrote that Comet Hale-Bopp appears to be chemically heterogeneous. These reports gave us a solid observational argument to study CO activity at different latitudes.

### 3.3. Results for CO activity

The integrated CO activity  $F_{CO}$  of Hale-Bopp is compared with observations. Activity is calculated through integration over the whole spherical nucleus

$$F_{CO} = f_a \frac{2\pi}{\tau_r} R^2 \int_{-\pi/2}^{\pi/2} d\theta \cos(\theta) \int_0^{\tau_r} dt q_{CO}(\theta, t). \quad (26)$$

$R$  is its radius, under the assumption that the comet is spherically symmetric. The fraction  $f_a$  of active surface areas is employed to fit the observations with the calculated production curves. This approach is commonly used although it might not always be stated.  $q_{CO}$  denotes the CO flux from a latitude  $\theta$  at time  $t$  at the surface.

For a thermal conductivity of  $0.01 \text{ W m}^{-1} \text{ K}^{-1}$  the CO production curve is shown in Fig. 3. It is assumed that the active CO spots are distributed over the whole nucleus. The spherical nucleus is divided in latitudinal direction into stripes with a thickness of 25°. The obliquity of the comet was set to 84° and the argument of the sub-solar meridian  $\Phi$  had a value of 105°. Apparently, the model is not able to reproduce the CO production rates of Biver et al. (2002). Only close to perihelion, the model seems to fit the observations.

This result is in agreement with previous reports. So far only Enzian (1999) and Capria et al. (2002) were able to present good fits of the CO observations, however, only over a limited heliocentric distance from  $-7$  to 4 AU. Both groups assumed a certain amount of CO gas trapped in amorphous ice, a certain amount of CO bulk ice to be present, and a certain amount of CO sublimating only when water ice sublimates. The latter mechanism was proposed by Capria et al. (2002). A similar assumption on the existence of amorphous ice was also made in Prialnik (1997a) and Prialnik (1997b).

Recent observational findings concerning the chemical heterogeneity (Lederer and Campins, 2002; Bockelée-Morvan et al., 2009) and a CO jet at a latitude of 20° (Bockelée-Morvan et al., 2009) indicate that cometary activity might be localized. Therefore, the CO activity of Hale-Bopp at different latitudes is investigated.

In Fig. 4, CO activity along the pre-perihelion branch is depicted. This result indicates that confining CO activity on the positive hemisphere above  $+10^\circ$  could fit the observations. The CO activity for different latitudinal heights along the post-perihelion branch is depicted in Fig. 5. It is apparent that a very good fit for the post-perihelion CO data of Biver et al. (2002) is obtained if CO activity is confined to the positive hemisphere above  $+10^\circ$  as in the pre-perihelion case. The result of such a scenario is displayed in Fig. 6.

The model is able to fit the CO observations of Biver et al. (2002) very well over the whole measured heliocentric distance starting at  $-7$  AU pre-perihelion to almost 15 AU post-perihelion. The fraction of active surface elements  $f_a$  was set to 0.75. The restriction to northern hemisphere CO sublimation is consistent with the CO jet at a latitude of  $20^\circ$  as reported by Bockelée-Morvan et al. (2009) for the observations at 11 March 1997, which was close to perihelion on the pre-perihelion branch. At around  $-2$  AU pre-perihelion the model approximates the local peak in the observations by a plateau.

### 3.4. Results for water activity

The water production curve for the best CO scenario of the previous section is depicted in Fig. 7. It is assumed that the positive hemisphere above  $10^\circ$  is active in water and CO while the remaining nucleus surface is still outgassing water vapor but not CO. The model is able to reproduce the general trend of the water observations throughout the orbit. The fraction of active surface elements  $f_a$  is about 0.25. This result is in agreement with Kührt (1999). Our fit of the water observations is slightly better than that presented in Enzian et al. (1998), Enzian (1999), and Capria et al. (2002). These groups argue that beyond 4 AU pre-perihelion water activity could only be due to icy grains in the coma while around perihelion nucleus activity is mainly responsible for the observed water activity of Hale-Bopp. Enzian et al. (1998) gave an estimate of the water activity of icy grains in the coma. The water production curve of that estimate seems to fit the water observations beyond 4 AU on the pre-perihelion branch. Along the post-perihelion branch, the water production rates, however, could not be reproduced with the assumption of extended water sources as proposed by Enzian et al. (1998).

In a recent article, Lederer et al. (2009) analyzed Hale-Bopp data with a Monte Carlo model which indicates that extended sources due to icy grains in the coma might contribute to water activity. The simulations were performed on data from April 22–26, 1997.

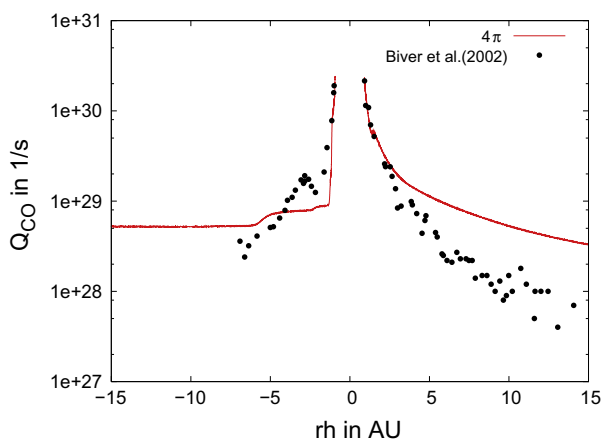


**Fig. 3.** CO production curve plotted as function of heliocentric distance. The curve is calculated by integration over the whole spherical nucleus. The fraction of active surface elements was about 0.25. The CO curve fits the CO data of Biver et al. (2002) only close to perihelion well.

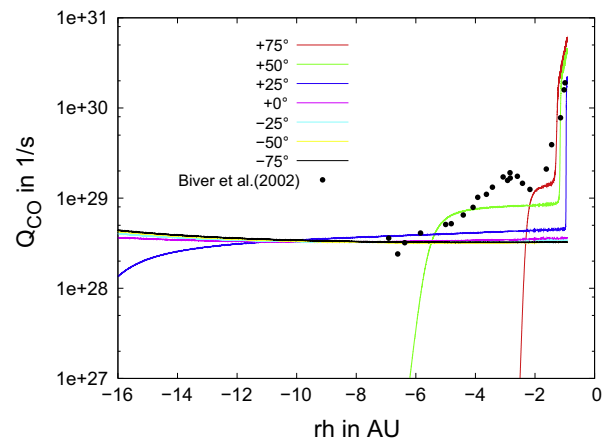


**Fig. 4.** Similar CO plot as in Fig. 3. The CO production of seven latitudinal stripes with thickness of  $25^\circ$  are presented along the pre-perihelion branch. The CO data of Biver et al. (2002) could be fitted if CO activity is confined to the positive hemisphere above a latitude of  $+10^\circ$ .

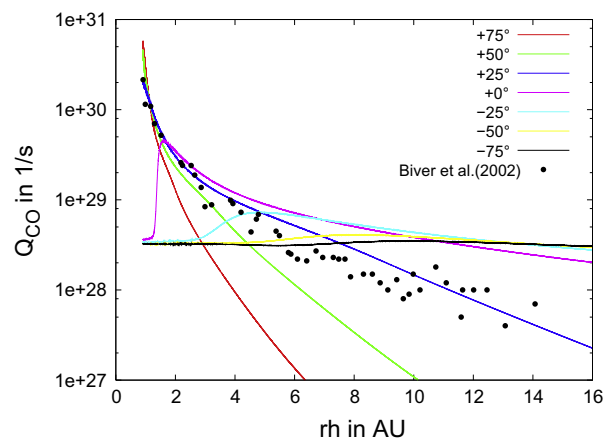


**Fig. 5.** Similar CO plot as in Fig. 4 for the post-perihelion branch. The CO data of Biver et al. (2002) along the post-perihelion branch could be fitted if CO activity is confined to the positive hemisphere above a latitude of  $+10^\circ$  as in the pre-perihelion case of Fig. 4.

At that time the comet was at the beginning of its post-perihelion branch.

Currently, it is difficult to judge to what extent cometary water activity could be due to extended sources and whether these sources contribute significantly to the observed water activity of this comet on its whole orbit or whether it is only a transient effect. It is also conceivable to achieve better agreement between the model calculations and the observed water activity of Hale-Bopp by fine-tuning the placement of active areas and their size, the spin pole vector, and by abandon the assumed spherical nucleus shape.

### 3.5. Results for different values of the argument $\Phi$ of the sub-solar meridian at perihelion

The illumination of a surface area on the nucleus depends according to Sekanina (1979) on the angle between the equatorial plane of the comet and the orbit plane, e.g. obliquity of the comet, and the argument  $\Phi$  of the sub-solar meridian at perihelion. These values enter the calculation of the solar zenith angle  $\zeta$  according to Eqs. (13) and (14). Unfortunately, these values are not so well constrained but they clearly influence the outgassing pattern of the nucleus.

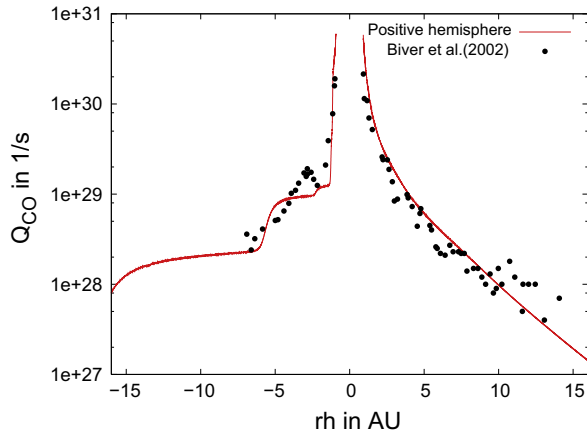


**Fig. 6.** Similar CO plot as in Fig. 3. The CO production curve is integrated over the positive hemisphere above  $10^\circ$ . The fraction of active surface elements was 0.75. The CO data of Biver et al. (2002) are well reproduced along the pre-perihelion branch and remarkably well along the whole post-perihelion branch covering a heliocentric distance from 1 AU to almost 15 AU. The local peak at around  $-2$  AU is approximated by a plateau.

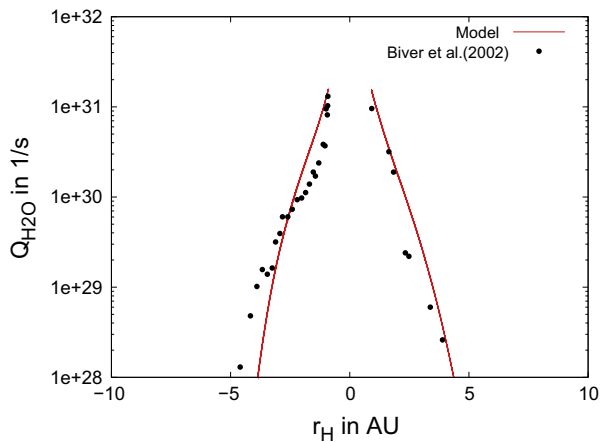


**Fig. 7.** Water production curve of Hale-Bopp plotted as function of heliocentric distance. The production curve is obtained through integration over a spherical nucleus with a fraction of active surface elements of 0.25. CO activity takes place on the positive hemisphere above  $10^\circ$  according to the best fit scenario of Fig. 6 while water active surface areas are distributed over the whole nucleus. Beyond  $-4$  AU pre-perihelion the model is not able to reproduce well the water activity. From  $-4$  AU to the outgoing leg water activity is well reproduced. This can be even improved if the fraction of active surface elements is reduced.

This should briefly be demonstrated for CO. The CO production curve for the best fit scenario of Section 3.3 is shown in Fig. 8 for an argument  $\Phi$  of  $105^\circ$  and  $95^\circ$ . Thus, changing  $\Phi$  by a value of  $10^\circ$  shifts the CO outgassing curve clearly. Hence, this parameter must be treated carefully when comparing simulations with observations.

#### 4. Discussion and conclusions

A thermophysical approach is presented to interpret the observations of Comet Hale-Bopp as reported by Biver et al. (2002).

The nucleus model accounts for heat conduction, heat advection, gas diffusion, sublimation, and condensation in an ice–dust matrix with moving boundaries. Surface erosion due to surface sublimation leads to a moving boundary which is resolved by applying a temperature remapping technique. This approach al-

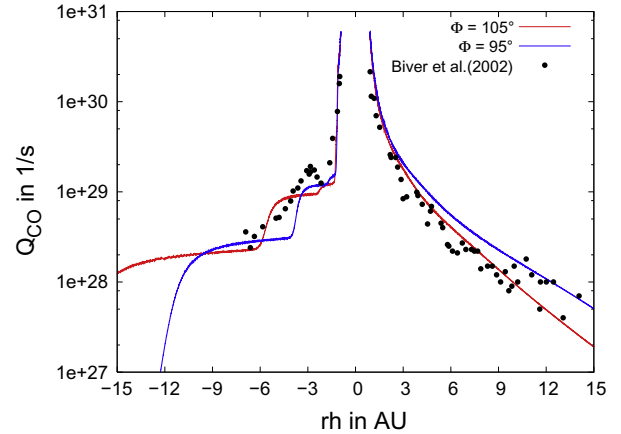


**Fig. 8.** Similar CO plot as in Fig. 6. The importance of the argument of the sub-solar meridian at perihelion  $\Phi$  for the CO production curve is demonstrated. Changing the argument by  $10^\circ$  shifts the outgassing curve, because the illumination conditions of the different latitudes throughout the orbit change. The obliquity was throughout this paper  $84^\circ$ . The argument  $\Phi$  and the obliquity enter the calculation of the solar zenith angle  $\zeta$  (Sekanina, 1979).

lows to take properly into account the loss in the internal energy of the eroded surface layers. Such moving boundary techniques are referred to as Stefan problems.

Our approach is guided by recent observational findings on important parameters controlling cometary activity. A low thermal conductivity (Kührt, 1999; Groussin et al., 2007), the obliquity of the rotation axis (Jorda et al., 1997), the chemical heterogeneity (Lederer and Campins, 2002; Bockelée-Morvan et al., 2009), and the CO jet at a latitude of  $20^\circ$  (Bockelée-Morvan et al., 2009) have been incorporated to calculate the water and CO activity.

For the first time, a thermal model is applied to the full data set of the water and CO production rates as reported by Biver et al. (2002). The data set covers the heliocentric range from  $-7$  AU pre- to 15 AU post-perihelion. The following results were obtained:

- The model is able to reproduce the water activity from  $-4$  AU pre- to the outgoing leg while it does not describe well the water activity beyond  $-4$  AU. It is assumed that the active spots are distributed randomly over the whole nucleus.
- The CO production curve fits the observations over the whole heliocentric distance starting at  $-7$  AU to 15 AU. Consistent with recent reports by Bockelée-Morvan et al. (2009) about a CO source at a latitude of  $20^\circ$  the best fit to the observations was obtained if CO activity is confined to the positive hemisphere above a latitude of  $10^\circ$ . Around  $-2$  AU pre-perihelion, the model approximates the local peak of the CO observations by a plateau.
- A low thermal conductivity of  $0.01 \text{ W K}^{-1} \text{ m}^{-1}$  is in good agreement with the Hale-Bopp observations.

In conclusion, currently there are two distinctly different approaches to model the outgassing pattern of Hale-Bopp for water and CO as reported by Biver et al. (2002). The approaches of Enzian (1999), Capria et al. (2002), and Prialnik (1997b) on the one hand. These models rely on the assumption that some form of amorphous ice must be present in the comet, that a certain percentage of CO must be trapped in the amorphous ice matrix which is released after phase transition, and that there is a certain percentage of CO bulk ice. On the other hand, the approach of this paper which tries to incorporate as many observational findings of the recent years as possible and which relies only on CO bulk ice.

Finally, the importance of the argument  $\Phi$  of the sub-solar meridian at perihelion for the CO production curve has also been demonstrated. The argument  $\Phi$  and the obliquity of the comet determine the distribution of the incoming solar energy on the nucleus surface. Changing  $\Phi$  by a value of  $10^\circ$  shifts the CO production curve clearly.

## Acknowledgments

We thank Detlef de Niem for discussions on the Stefan Problem. We are very grateful to B. Davidsson and H. Rickman for discussions on the thermal physics of comets. One of us (E.K.) would like to thank Prof. J. Geiss for fruitful discussions during a stay at the International Space Science Institute (ISSI) in Bern. We appreciate the valuable comments of B. Davidsson and an anonymous referee who helped to improve the paper.

## References

- Benkhoff, J., Spohn, T., 1991. Results of a coupled heat and mass transfer model applied to KOSI sublimation experiments. In: Kömle, N.I., Bauer, S.J., Spohn, T. (Eds.), *Theoretical Modelling of Comet Simulation Experiments*. Verlag der Österreichischen Akademie der Wissenschaften, Wien, pp. 31–47.
- Biver, N. et al., 1997. Long-term evolution of the outgassing of Comet Hale-Bopp from radio observations. *Earth Moon Planets* 78, 5–11.
- Biver, N. et al., 2002. The 1995–2002 long-term monitoring of Comet C/1995 O1 (Hale-Bopp) at radio wavelength. *Earth Moon Planets* 90, 5–14.
- Bockelée-Morvan, D., Rickman, H., 1997. C/1995 O1 (Hale-Bopp): Gas production curves and their interpretation. *Earth Moon Planets* 79, 55–77.
- Bockelée-Morvan, D., Henry, F., Biver, N., Boissier, J., Colom, P., Crovisier, J., Despois, D., Moreno, R., Wink, J., 2009. Interferometric imaging of carbon monoxide in Comet C/1995 O1 (Hale-Bopp): Evidence of a strong rotating jet. *Astron. Astrophys.* 505, 825–843.
- Capria, M.T., Coradini, A., De Sanctis, M.C., Orosei, R., 2000. CO emission mechanisms in C/1995 O1 (Hale-Bopp). *Astron. Astrophys.* 357, 359–366.
- Capria, M.T., Coradini, A., De Sanctis, M.C., 2002. C/1995 O1 Hale-Bopp: Short and long distance activity from a theoretical model. *Earth Moon Planets* 90, 217–225.
- Colom, P., Gérard, E., Crovisier, J., Bockel-Morvan, D., Biver, N., Rauer, H., 1997. Observations of the OH radical in Comet Hale-Bopp with the Nançay Radio Telescope. *Earth Moon Planets* 78, 37–43.
- Crank, J., 1984. *Free and Moving Boundary Problems*. Oxford University Press, New York.
- Crank, J., Gupta, R.S., 1972. A method for solving moving boundary problems in heat flow using cubic splines or polynomials. *J. Inst. Math. Appl.* 10, 296–304.
- Crovisier, J., Leech, K., Bockelée-Morvan, D., Lellouch, E., Brooke, T.Y., Hanner, M.S., Altieri, B., Keller, H.U., Lim, T., 1999. The spectrum of Comet Hale-Bopp as seen by ISO. In: Cox, P., Kessler, M. (Eds.), *The Universe as Seen by ISO*. ESA Special Publication, pp. 137–140.
- Davidsson, B.J.R., Skorov, Y.V., 2002b. On the light-absorbing surface layer of cometary nuclei: II. Thermal modeling. *Icarus* 159, 239–258.
- Davidsson, B.J.R., Skorov, Y.V., 2004. A practical tool for simulating the presence of gas comae in thermophysical modeling of cometary nuclei. *Icarus* 168, 163–185.
- Davidsson, B.J.R., Gutiérrez, P.J., Rickman, H., 2009. Physical properties of morphological units on Comet 9P/Tempel 1 derived from near-IR Deep Impact spectra. *Icarus* 201, 335–357.
- Enzian, A., 1999. On the prediction of CO outgassing from Comets Hale-Bopp and Wirtanen. *Space Sci. Rev.* 90, 131–139.
- Enzian, A., Cabot, H., Klinger, J., 1998. Simulation of the water and carbon monoxide production rates of Comet Hale-Bopp using a quasi 3-D nucleus model. *Planet. Space Sci.* 46, 851–858.
- Fanale, F.P., Salvail, J.R., 1984. An idealized short-period comet model – Surface insolation, H<sub>2</sub>O flux, dust flux, and mantle evolution. *Icarus* 60, 476–511.
- Fernández, Y.R., 2002. The nucleus of Comet Hale-Bopp (C/1995 O1): Size and activity. *Earth Moon Planets* 89, 3–25.
- Flammer, K.R., Mendis, D.A., Houpis, H.L.F., 1999. On the outgassing profile of Comet Hale-Bopp. *Astrophys. J.* 494, 822–827.
- Groussin, O., A'Hearn, M.F., Li, J.-Y., Thomas, P.C., Sunshine, J.M., Lisse, C.M., Meech, K.J., Farnham, T.L., Feaga, L.M., Delamere, W.A., 2007. Surface temperature of the nucleus of Comet 9P/Tempel 1. *Icarus* 187, 16–25.
- Grün, E., Gebhard, J., Bar-Nun, A., Benkhoff, J., Dueren, H., Eich, G., Hische, R., Huebner, W.F., Keller, H.U., Klees, G., 1993. Development of a dust mantle on the surface of an insolated ice–dust mixture – Results from the KOSI-9 experiment. *J. Geophys. Res.* 98, 15091–15104.
- Huebner, W.F., 2009. Origins of cometary materials. In: Balsiger, H., Altwegg, K., Huebner, W., Owen, T., Schulz, R. (Eds.), *Origin and Early Evolution of Comet Nuclei*. The International Space Science Institute, Bern, Switzerland, pp. 5–25.
- Jewitt, D., Senay, M., Matthews, H., 1996. Observations of carbon monoxide in Comet Hale-Bopp. *Science* 271, 1110–1113.
- Jorda, L., Rembor, K., Lecacheux, J., Colom, P., Colas, F., Frappa, E., Lara, L.M., 1997. The rotational parameters of HaleBopp (C/1995 O1) from observations of the dust jets at Pic du Midi observatory. *Earth Moon Planets* 77, 167–180.
- Kührt, E., 1999. H<sub>2</sub>O-activity of Comet Hale-Bopp. *Space Sci. Rev.* 90, 75–82.
- Lederer, S.M., Campins, H., 2002. Evidence for chemical heterogeneity in the nucleus of C/1995 O1 (Hale-Bopp). *Earth Moon Planets* 90, 381–389.
- Lederer, S.M., Campins, H., Osip, D.J., 2009. Chemical and physical properties of gas jets in comets: II. Modeling OH, CN and C<sub>2</sub> jets in Comet C/1995 O1 (Hale-Bopp) one month after perihelion. *Icarus* 199, 484–504.
- Mekler, Y., Prialnik, D., Podolak, M., 1990. Evaporation from a porous cometary nucleus. *Astrophys. J.* 356, 682–686.
- Prialnik, D., 1997a. A model for the distant activity of Comet Hale-Bopp. *Astrophys. J.* 478, 107–110.
- Prialnik, D., 1997b. Modelling gas and dust release from Comet Hale-Bopp. *Earth Moon Planets* 77, 223–230.
- Seiferlin, K., 1991. The thermal conductivity of porous ice with application to KOSI sample material: A review. In: Kömle, N.I., Bauer, S.J., Spohn, T. (Eds.), *Theoretical Modelling of Comet Simulation Experiments*. Verlag der Österreichischen Akademie der Wissenschaften, Wien, pp. 9–66.
- Seiferlin, K., Kömle, N.I., Kargl, G., Spohn, T., 1996. Line heat-source measurements of the thermal conductivity of porous H<sub>2</sub>O ice, CO<sub>2</sub> ice and mineral powders under space conditions. *Planet. Space Sci.* 44, 691–704.
- Sekanina, Z., 1979. Fan-shaped coma, orientation of rotation axis, and surface structure of a cometary nucleus. I – Test of a model on four comets. *Icarus* 37, 420–442.
- Skorov, Y.V., Kömle, N.I., Keller, H.U., Kargl, G., Markiewicz, W.J., 2001. A model of heat and mass transfer in a porous cometary nucleus based on a kinetic treatment of mass flow. *Icarus* 153, 180–196.
- Spohn, T., Benkhoff, J., 1990. Thermal history models for KOSI sublimation experiments. *Icarus* 87, 358–371.
- Spohn, T., Benkhoff, J., Klinger, J., Grün, E., Kochan, H., 1989. Thermal modelling of two KOSI comet nucleus simulation experiments. *Adv. Space Sci.* 9, 127–131.
- Stefan, J., 1891. Über die Theorie der Eisbildung, insbesondere über die Eisbildung im Polarmeere. *Ann. Phys. Chem.* 42, 269–286.
- Steiner, G., Kömle, N.I., 1991. Thermal budget of multicomponent porous ices. *J. Geophys. Res.* 96, 18897–18902.
- Stern, S.A., Colwell, W.B., Festou, M.C., Tamblyn, P.M., Parker, J.W., Slater, D.C., Weissman, P.R., Paxton, L.J., 1999. Comet Hale-Bopp (C/1995 O1) near 2.3 AU postperihelion: Southwest ultraviolet imaging system measurements of the H<sub>2</sub>O and dust production. *Astrophys. J.* 118, 1120–1125.
- Stöffler, D., Duren, H., Knolker, J., Hische, R., Bischoff, A., 1991. Cometary analogue material – Preparation, composition, and thin section petrography. *Geophys. Res. Lett.* 18, 285–288.
- Vasundhara, R., Chakraborty, P., 1999. Modeling of jets from Comet Hale-Bopp (C/1995 O1): Observations from the Vainu Bappu Observatory. *Icarus* 140, 221–230.
- Weaver, H.A., Feldman, P.D., A'Hearn, M.F., Arpigny, C., Brandt, J.C., Stern, S.A., 1999. Post-perihelion HST observations of Comet Hale-Bopp (C/1995 O1). *Icarus* 141, 1–12.